A Ru(II) Polypyridyl Complex Bearing Aldehyde Functions as a Versatile Synthetic Precursor for Long-Wavelength Absorbing Photodynamic Therapy Photosensitizers

Johannes Karges, Franz Heinemann, Federica Maschietto, Malay Patra, Olivier Blacque, Ilaria Ciofini, Bernhard Spingler, Gilles Gasser

A Ru(II) Polypyridyl Complex Bearing Aldehyde Functions as a Versatile Synthetic Precursor for Long-Wavelength Absorbing Photodynamic Therapy Photosensitizers

Johannes Karges,[a,#] Franz Heinemann,[a,b,#] Federica Maschietto,[c] Malay Patra,[b,d] Olivier Blacque,[b] Ilaria Ciofini,[c] Bernhard Spingler,[b,] and Gilles Gasser[a,*]*

[a] Chimie ParisTech, PSL University, CNRS, Institute of Chemistry for Life and Health Sciences, Laboratory for Inorganic Chemical Biology, 75005 Paris, France.

[b] Department of Chemistry, University of Zurich, Winterthurerstrasse 190, 8057 Zurich, Switzerland.

[c] Chimie ParisTech, PSL University, CNRS, Institute of Chemistry for Life and Health Sciences, Theoretical Chemistry and Modelling, 75005 Paris, France.

[d] Please note the new address: Department of Chemical Sciences, Tata Institute of Fundamental Research, Colaba, Mumbai 400005, India.

# These authors have contributed equally to the work.

*Email: spingler@chem.uzh.ch; Tel. +41 44 63 546 56; gilles.gasser@chimieparistech.psl.eu; Tel. +33 1 44 27 56 02.

ORCID-ID:

Johannes Karges: 0000-0001-5258-0260

Franz Heinemann: 0000-0001-9590-443X

Federica Maschietto: 0000-0002-5995-2765

Malay Patra: 0000-0003-3373-6762

Olivier Blacque: 0000-0001-9857-4042

Ilaria Ciofini: 0000-0002-5391-4522

Bernhard Spingler: 0000-0003-3402-2016

Gilles Gasser: 0000-0002-4244-5097

Keywords

Anticancer, Medicinal Inorganic Chemistry, Metals in Medicine, Photosensitizer, Photodynamic Therapy.

Graphica Abstract

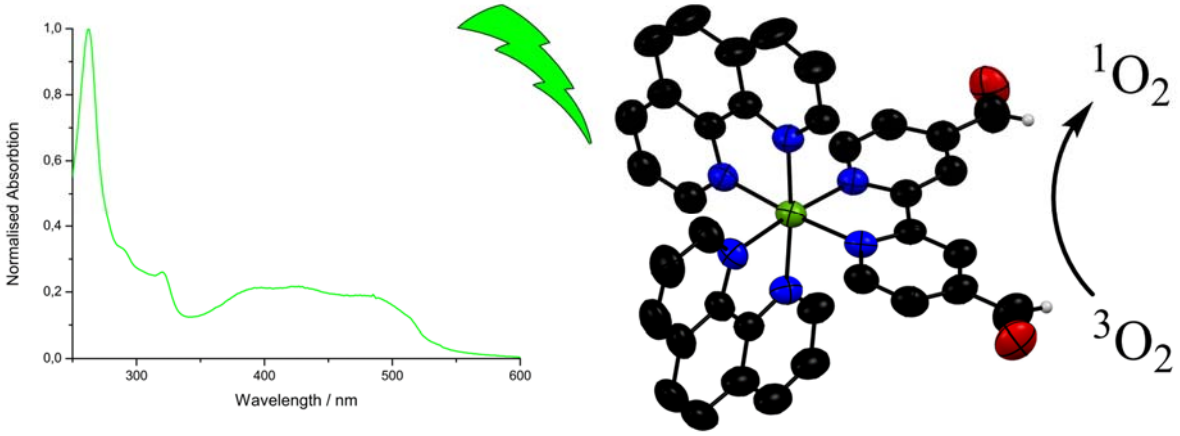

ABSTRACT

The use of Photodynamic Therapy (PDT) for the treatment of several kinds of cancer as well as bacterial, fungal or viral infections has received increasing attention during the last decade. However, the currently clinically approved photosensitizers (PSs) have several drawbacks, including photobleaching, slow clearance from the organism and poor water solubility. To overcome these shortcomings, much effort has been made in the development of new types of PSs, such as Ru(II) polypyridyl complexes. Nevertheless, most studied Ru(II) polypyridyl complexes have a low absorbance in the spectral therapeutic window. In this work, we show that, by carefully selecting substituents on the polypyridyl complex, it is possible to prepare a complex absorbing at much higher wavelength. Specifically, we report on the synthesis and in-depth experimental and theoretical characterisation of a Ru(II) polypyridyl complex (complex **3**) combining a shift in absorbance towards the spectral therapeutic window with a high $^1O_2$ production. To overcome the absence or poor selectivity of most approved PS into targeted cells/bacteria, they can be linked to targeting moieties. In this line, compound **3** was designed with reactive aldehyde groups, which can be used as a highly versatile synthetic precursor for further conjugation. As a proof of concept, **3** was reacted with benzylamine and the stability of the resulting conjugate **4** was investigated in DMSO, PBS and cell media. **4** showed an impressive ability to act as a PDT PS with no measurable dark cytotoxicity and photocytotoxicity in the low micromolar range against cancerous HeLa cells from 450 nm up to 540 nm.

1. INTRODUCTION

Photodynamic Therapy (PDT) is a medical technique for the treatment of several kinds of cancer (i.e. lung, bladder, oesophageal and brain cancer) as well as bacterial, fungal or viral infections. The mechanism of action of PDT relies on a combination of a photosensitizer (PS), oxygen and light. To date, the majority of investigated and approved PS are based on a tetrapyrrolic scaffold (i.e. porphyrins, chlorins), leading, generally, to similar properties and therefore to similar drawbacks. In the context of PDT, these shortcomings are 1) poor water solubility; 2) photobleaching; 3) low selectivity for cancer tissue and 4) slow clearance from the body causing photosensitivity to the patients. To overcome these limitations, there is a need for modification of existing PSs or the development of new classes of PSs.[1-11] Among other classes of compounds, the development of Ru(II) polypyridyl complexes is receiving increasing attention due to their excellent properties (i.e. high water solubility, high chemical stability and photostability, intense luminescence, large Stokes shifts, high $^1O_2$ production). As a highlight, TLD-1433 from the McFarland group has just completed phase I clinical trial as a PDT agent against bladder cancer.[8] However, most synthesised and studied Ru(II) polypyridyl complexes lack absorbance in the spectral therapeutic window (600-900 nm). Therefore, a lot of efforts have recently been made towards the development of Ru(II)-based PDT PSs showing a red shift in absorbance with respect to parent compounds.[9-14] As a highly investigated class of compounds, $[Ru(phen)_3]^{2+}$ derivatives have been studied as PDT PSs.[15-18] Several examples have shown that the photophysical properties, including absorption, emission as well as excited states lifetimes can be influenced by choice of the coordinated ligands.[5, 9, 11, 13, 19]

Next to suitable photophysical properties, the biological abilities of a PS including, for example, cellular localisation or mechanism of cellular uptake, play a predominant role in the efficiency of the treatment. As a model complex, $[Ru(phen)_3]^{2+}$ was found to be strongly binding to the minor groove of the DNA.[20, 21] By causing oxidative stress upon light irradiation, the replication machinery and integrity of the genetic material can be damaged.[13-15, 22, 23] To improve the PDT ability of a PS, the biological (e.g. cellular uptake and localisation) and pharmacological properties can be tuned by functionalisation with a different moieties. These additional fragments can be 1) a biologically active molecule which acts through a different mechanism than the PS [24-26]; 2) a luminescent moiety for imaging[27]; 3) hydrophilic or hydrophobic groups to change the lipophilicity to increase cellular uptake and/or change the cellular localisation[12, 28] or 4) a targeting moiety to selectively deliver the PS to

tumor/bacteria.[14, 29, 30] Herein, we have designed a Ru(II) polypyridine complex bearing two aldehyde functional groups (complex **3**, Scheme 1). As demonstrated in numerous examples,[31, 32] aldehydes are known to be very reactive groups, that can be used versatilely in organic synthesis. Importantly, it has already been shown that small organic molecule functionalized with an aldehyde group can be linked to peptides or proteins at room temperature in biological buffers.[33-35]

Herein, we report on the synthesis of the Ru(II) polypyridine complex **3** as a synthetic precursor for long-wavelength PDT. We have investigated experimentally as well as by theoretical calculations the photophysical properties of **3**. As a proof of concept of its high versatility as a synthetic precursor for conjugations, we condensated the aldehyde groups with benzylamine. The stability of the conjugate was tested in DMSO, PBS and cell media. As shown below, the conjugate **4** is highly toxic to cervical cancer HeLa cancer cells upon light irradiation (450, 480, 510 and 540 nm) with IC_{50} values in the low micromolar range and, importantly, no measurable dark cytotoxicity.

2. RESULTS AND DISCUSSION

2.1. Synthesis and Characterisation

Complex **3** was synthesised as described in Scheme 1. To the best of our knowledge, the synthesis of **3** has not been reported yet, whereas the syntheses of the ligand intermediates (*E*,*E*')-4,4'-bis(*N*,*N*-dimethylaminovinyl)-2,2'-bipyridine **1** and 2,2′-bipyridine-4,4′-dicarboxaldehyde **2** were previously published.[36] However, here, slightly different experimental procedures were utilized. **1** was synthesised by an enamination reaction with *tert*-butoxy bis(dimethylamino) methane, also known as the Bredereck reagent. Subsequently, **2** was formed by an oxidative cleavage of the double bond with sodium periodate. The Ru(II) precursor dichlorobis(1,10-phenanthroline)ruthenium(II) $RuCl_2(phen)_2$ was synthesised as previously published.[37] Finally, the desired complex **3** was prepared by complexation of $RuCl_2(phen)_2$ with **2**. The identity of the complex was confirmed by ^1H, ^{13}C-NMR and ESI-HRMS and the purity by HPLC and elemental analysis (Figure S1-S4).

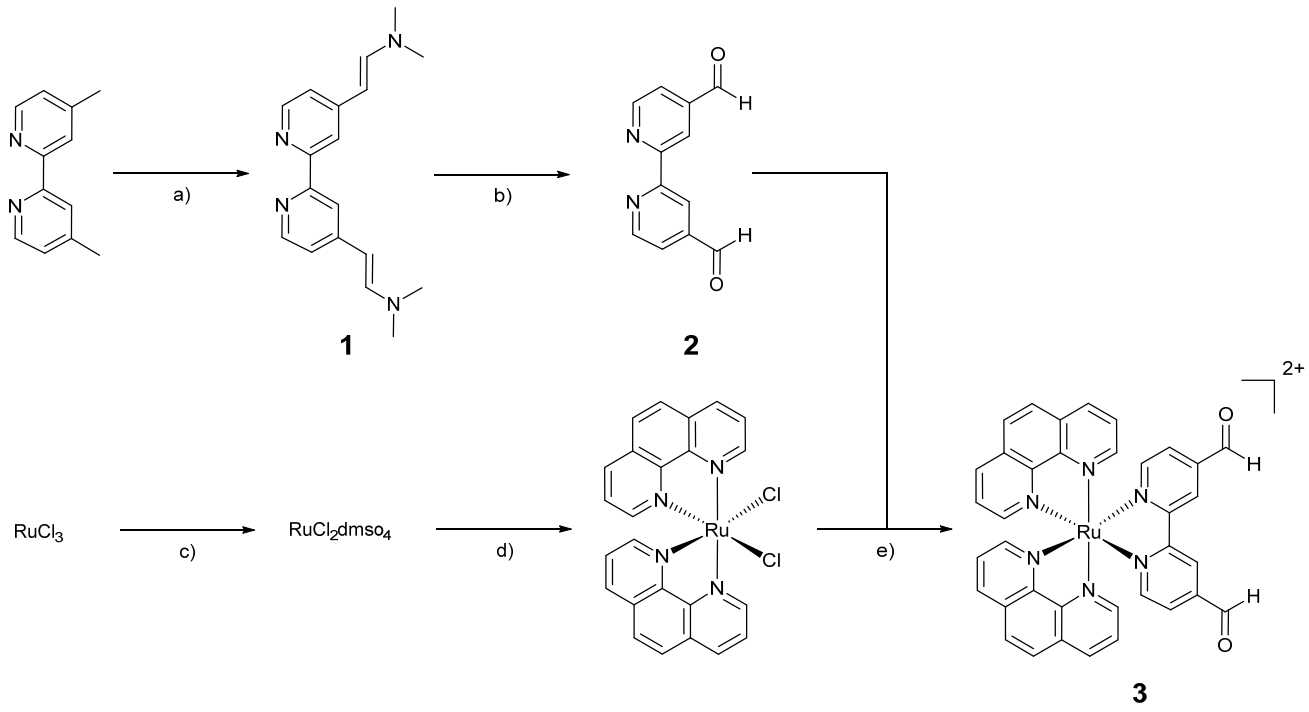

Scheme 1. Synthesis of the desired complex **3**. a) *tert*-butoxy bis(dimethylamino)methane/Bredereck reagent, DMF, 140 °C for 24 h under N_2 atmosphere, 79%; b) $NaIO_4$, THF/H_2O (1:1), 50 °C for 20 h under N_2 atmosphere, 78%; c) EtOH, reflux for 3h, DMSO, 150°C for 2 h, 86%; d) 1,10-phenanthroline, LiCl, DMF, reflux overnight under N_2 atmosphere, 63%; e) EtOH/H_2O (1:1), reflux for 18 h under N_2 atmosphere, 69%.

2.2. X-ray Crystallography

Two batches of crystals of complex **3** were obtained from vapour diffusion of acetone/chloroform (a) and acetonitrile/tetrahydropyran (b).[38] Single crystal X-ray diffraction studies carried out on a selected crystal from each batch gave different cell parameters. Crystal data, structure refinement parameters and molecular structures of **3a** and **3b** are presented in Table S1 and Figures 1 and S5. The crystals grown from acetone/chloroform (**3a**) contain a ruthenium(II) dicationic complex, two PF_6^- counterions and two solvent molecules of chloroform. The crystals of **3b** were all very flat and twinned along the smallest direction, it was physically not possible to get rid of the twinning but the diffraction intensities were successfully integrated according to the non-merohedral twin law (1 -0.559 -0.180 0 -1 0 0 0 -1) in the direct space. The structure of **3b** was solved but some regions of severely disordered solvent molecules could not be refined with a reasonable modelling. The SQUEEZE routine in PLATON[39] was used to take into account the solvent contribution to the calculated structure factors: 125 electrons were found in the P1 unit cell, which were considered as two molecules of $C_5H_{10}O$ and one molecule of CH_3CN. In both structures, the Ru(II) ion is coordinated by two phenantroline ligands and one substituted bipyridine ligand through the N atoms in a distorted octahedral geometry. Despite all aromatic rings present in the dicationic molecules, there are no π…π interactions in the crystal structures, the supramolecular structures are formed by weak C-H…O and C-H…F interactions.

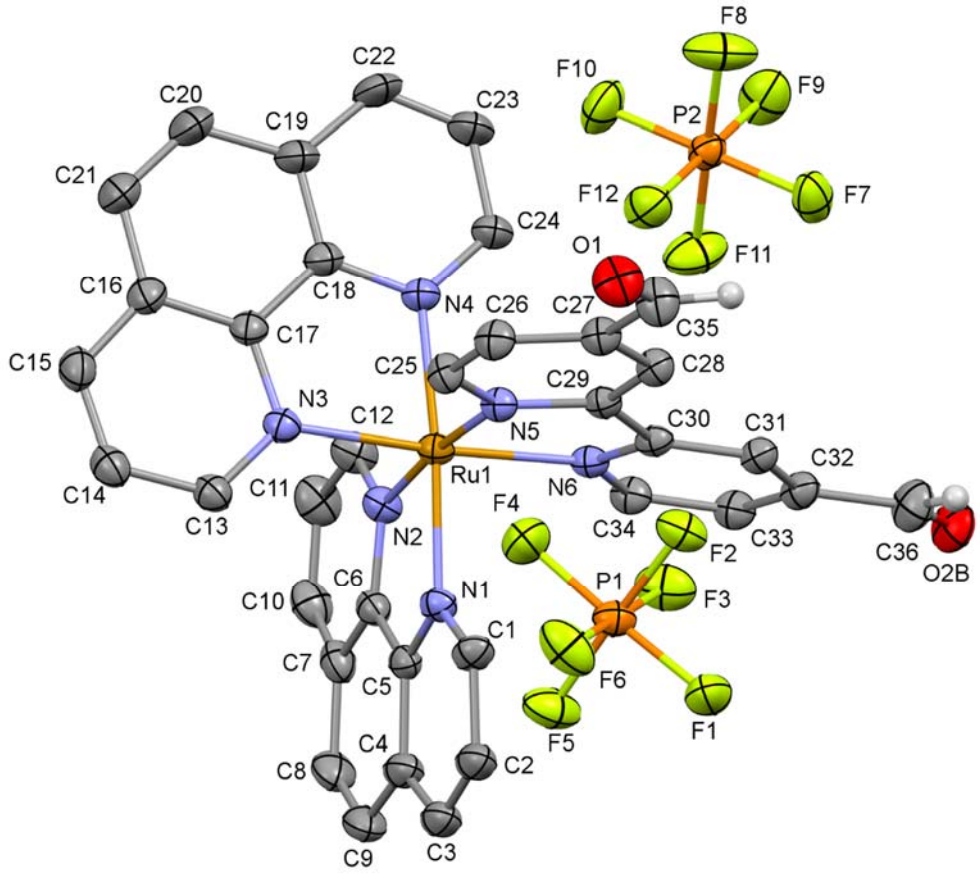

Figure 1. Molecular structure of **3b**. The thermal ellipsoids are drawn at the 30 % probability level and selected H atoms are omitted for clarity.

2.3. Photophysical properties

To evaluate the potential of complex **3** as a PDT PS, we performed photophysical measurements. Due to the direct influence of the wavelengths used in PDT on the light penetration depth into tissue, the absorption of the compound was measured in CH_3CN. Based on the comparison with similar Ru(II) polypyridyl complexes, the absorption bands (Figure 2) were experimentally assigned.[40, 41]

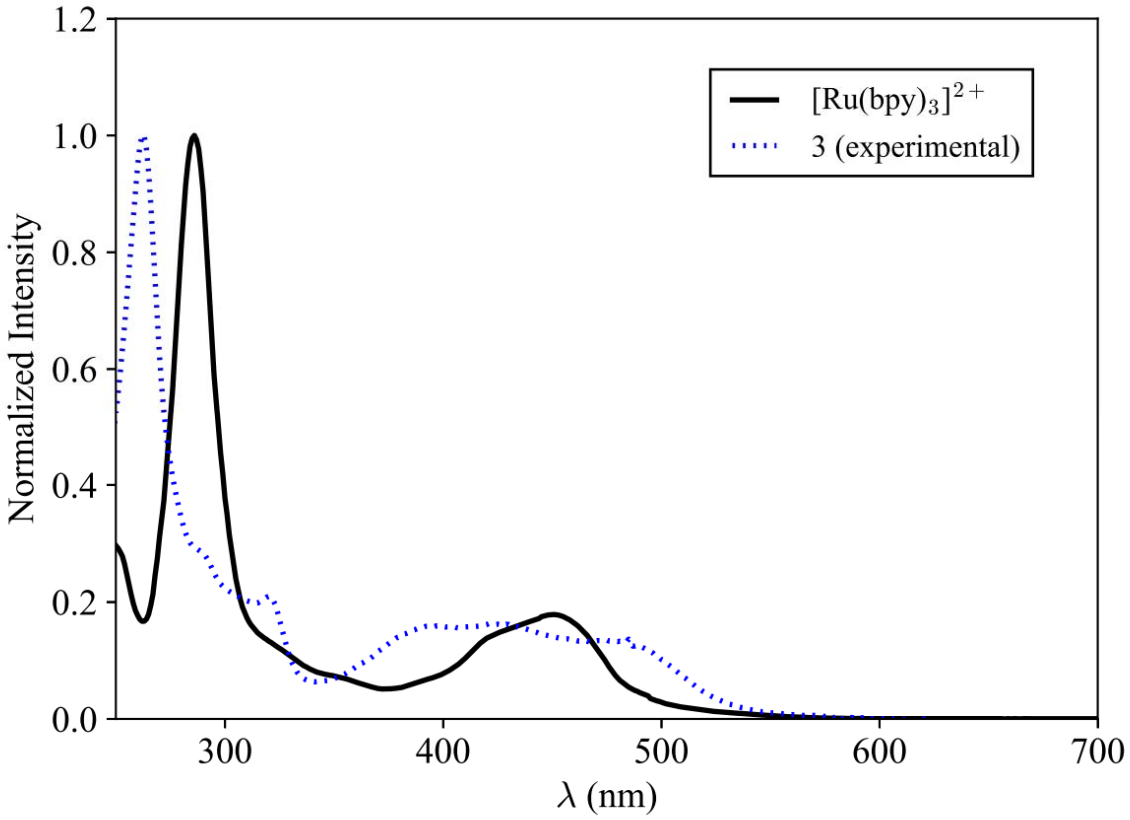

Figure 2. Normalised absorption spectrum of **3** and $[Ru(bipy)_3]^{2+}$ in CH_3CN.

The highest energy bands were attributed to ligand centered (LC) transitions while lowest energy absorption bands were assigned to a metal-to-ligand charge transfer (MLCT) transition. Comparison (Figure 2) with the prototype complex, $[Ru(bipy)_3]^{2+}$, enables to show that the MLCT transition, occurring at 450 nm in the latter[42] is red-shifted of roughly 35 nm in the case of **3** with an absorption tail towards the therapeutic spectral window (600-900 nm). At this stage, it is important to highlight that, despite the low absorption in the therapeutic spectral window of the complex, it is still possible to envision an irradiation at these wavelength, as demonstrated by McFarland.[8]

The experimental assignment was confirmed by Density Functional Theory (DFT) and Time Dependent DFT (TDDFT) calculations (see also the Computational Details section). The full list of computed transition energies and corresponding intensities (oscillator strength, f) is given in SI (Table S2) while the corresponding computed spectrum, obtained by the means of a Gaussian convolution of the vertical transitions represented as vertical bars is reported, together with experimental spectrum, in Figure 2. Overall, while bands at high energies are

quantitatively reproduced by TD-DFT calculations, a shift towards higher energies is observed for the broad band observed between 400 and 500 nm which is thus only qualitatively predicted.

Indeed, the first intense electronic transition is computed at 447 nm and corresponds to the third excited state, the first two ES (computed at 518 and 489 nm) being only very weakly absorbing. Analysis of the nature of computed transitions allows to confirm the experimental attribution of the main bands. In particular, the band observed –and computed- at 262 nm corresponds essentially to an intense LC transition while several transitions with non-negligible intensity contribute to the lowest energy band. Among these transitions, the lowest energy one (ES1, in Figure 3) as well as the most intense ones (ES3 and ES6, Figure 3) have a clear Metal to Ligand Charge Transfer (MLCT) character as highlighted by the analysis of the excited state density. The computed difference between excited (ES) and ground state (GS) densities (reported in Figure 3) allows to visualize the regions corresponding to an increase or a depletion of electronic density upon excitation. These regions, depicted in yellow and blue, respectively, basically cover the donor/acceptor moieties of the molecule involved in each transition. In order to provide a more quantitative information concerning the CT character associated to each transition, a charge transfer length (D_{CT})[43-45] can be computed from these density difference distributions as the distance between the barycentres of the density depletion and increase zones. These barycenters, represented as yellow and blue dots in Figure 3, provide a simple picture of the hole and the electron position for each transition. As depicted in figure 3, for these transitions the hole is essentially localized on the metal while an electron density increase on the ligand carrying the aldhehydes substituents as expected in the case of a MLCT transition.

The emission of these complexes in CH_3CN was determined upon excitation at 355 nm. Complex **3** shows an emission maximum at 710 nm (Figure S6), which results in a large Stokes shift implying minimal inference between excitation and luminescence. Consequently, the luminescence quantum yield (Φ_{em}) of the complex was determined upon excitation in CH_3CN at 355 nm and compared with the prototype complex $[Ru(bipy)_3]^{2+}$ in CH_3CN (Φ_{em}=0.059 %)[46]. The value was found to be 0.011 %, in a range similar to that of other Ru(II) complexes.[47-49] Additionally, the luminescence lifetime was determined upon excitation at 355 nm in CH_3CN. Compound **3** has a lifetime of 578 ns in a degassed and of 120 ns (Figure S7) in an air saturated CH_3CN solution. The obtained values are in the same range as compared with other Ru(II)-complexes.[47-49] More importantly, these values show that the presence of

oxygen has a significant influence on the lifetime of the excited state. This indicates that molecular oxygen can interact with the triplet state of the complex.

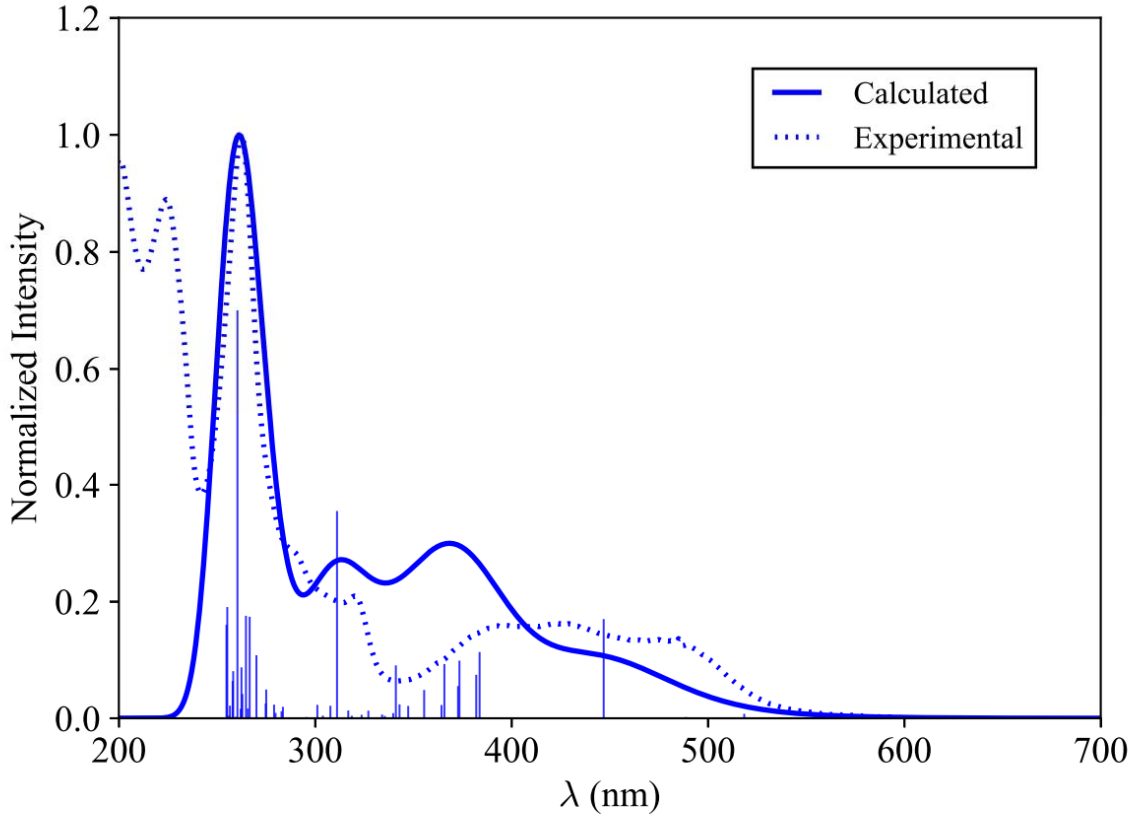

Figure 3. Experimental and computed absorption spectra of **3**. Vertical bars correspond to computed vertical transitions while the computed spectrum was obtained by a Gaussian convolution (see Computational Details).

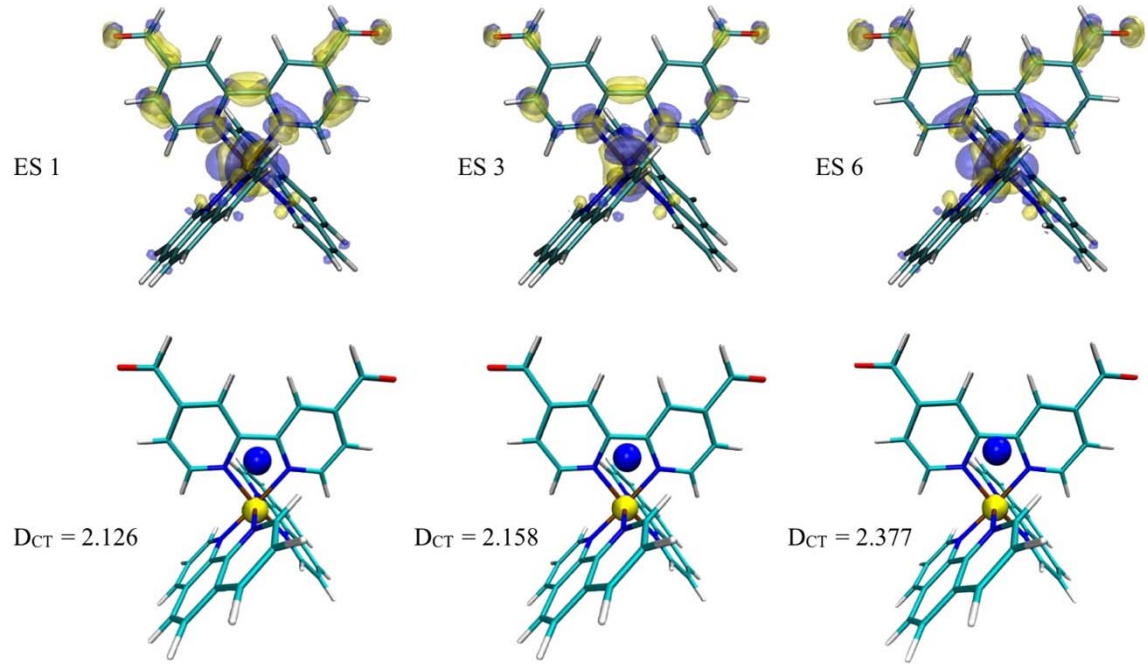

Figure 4. Plots representing the difference in density between ES and GS computed for the first (ES=1, λ=518 nm, f=0.01 a.u.), the third (ES=3 λ=447 nm, f=0.248 a.u.) and the sixth (ES=6; λ=384 nm, f=0.166 a.u.) vertical transitions and are shown together with the corresponding D_{CT} values (in Å). Yellow regions are characterized by an increase in density upon excitation while blue ones show a decrease in electron density. Barycenters of the density increase/decrease density distributions are represented in blue and yellow, respectively. Atoms colorscheme: C-green; H-white; N-blue; O-red, Ru-brown.

2.4. Singlet oxygen generation

The drastic decrease of the excited state lifetimes of complex **3** in a degassed in comparison to an air-saturated solution indicates that the excited state of **3** is able to interact with molecular oxygen ($^3O_2$). Having this in mind, we performed a quantification of the singlet oxygen ($^1O_2$) production. The $^1O_2$ quantum yields were determined by two methods, as previously published by our group:[50, 51] 1) direct method by measurement of the luminescence of $^1O_2$ at 1270 nm, 2) indirect method by measurement of the variation in absorbance of the reporter molecule imidazole (in CH_3CN) or histidine (in PBS). The obtained values were compared with a reference, namely phenalenone ($\Phi(^1O_2)_{phenaleone}$=0.95) in CH_3CN [52] and $[Ru(bipy)_3]Cl_2$ ($\Phi(^1O_2)_{Ru(bipy)3Cl2}$=0.22) in a aqueous solution.[47] The results obtained are shown in Table 2. Compound **3** was found to exhibit an about 2.5 times higher singlet oxygen production in CH_3CN than in an aqueous solution. This observation as well as the data itself is comparable with previously reported data on Ru(II) complexes investigated as PDT PSs.[12, 13, 28, 47]

Table 2. Singlet oxygen quantum yields ($\Phi(^1O_2)$) in CH_3CN and aqueous solution determined by direct and indirect methods by excitation at 450 nm. Average of three independent measurements, +-10%.

Compound	**CH_3CN Direct**	**CH_3CN Indirect**	**D_2O Direct**	**PBS Indirect**
3	0.64	0.69	0.23	0.27

2.5. Conjugation of the synthetic precursor 3 to benzylamine

After having fully assessed the photophysical properties of the Ru precursor **3**, we investigated the possibility of conjugation of the Ru(II) polypyridine complex **3** to other molecules through the reactivity of the aldehyde groups. So far, bipyridine derivatives bearing aldehyde functional groups have been used for conjugation via imines,[53-59] Wittig reactions,[60-64] Baylis–Hillman reactions,[65] Knoevenagel condensations[66-68] or aldol condensations[69]. To evaluate the potential of **3** to act as a synthetic precursor, we synthesised, as a proof of concept, an imine adduct via condensation of the aldehyde with the amine group of benzylamine (Scheme 2). The identity of the synthesised conjugate was confirmed by ^1H, ^{13}C-NMR and ESI-MS (Figure S8-S10).

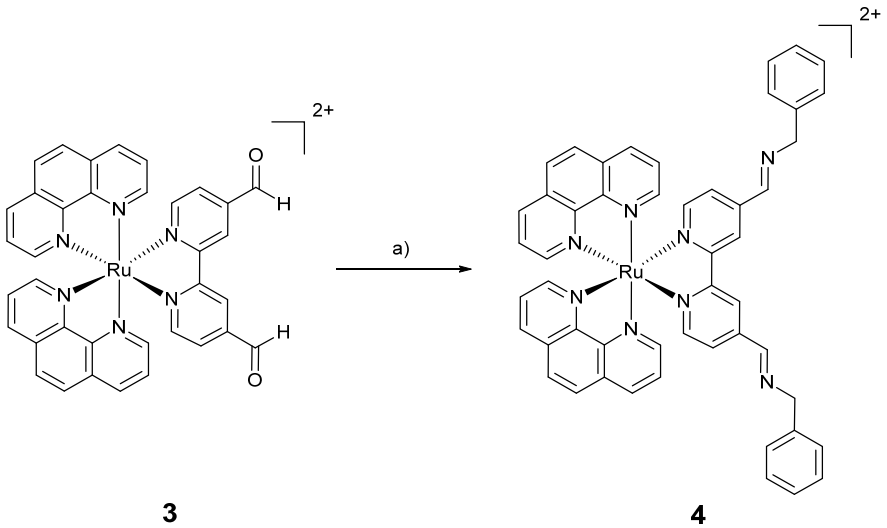

3 **4**

Scheme 2. Synthesis of conjugate **4**. a) benzylamine, EtOH, 50°C for 2 h under N_2 atmosphere, 54%.

TD-DFT spectrum of compound **4** (computed in CH_3CN for the sake of consistency and reported in SI as Figure S11) predicts a slight enhancement of the absorbance with respect to

compound **3** in the 400-500 nm region together with a slight blue shift of this absorption band. The most intense electronic transition contributing to this band is indeed blue shifted of roughly 20 nm. Analogously to what computed for compound **3**, this electronic transition corresponds to third excited state (ES3) as reported in Table S3 and Figure S12. The nature of the first three transitions giving rise to the broad band in the 400-500 nm region is indeed unchanged with respect to compound **3**, all having a MLCT character. The imine groups seem to act as weak acceptors, the MLCT transitions being directed from the metal center towards the ligand carrying the imine substituents in analogy with the behavior observed for compound **3**.

2.6. Stability of the conjugate 4

A crucial parameter for the use of a compound for any kind of biological application is its stability in a biological environment. As a first experiment, we have investigated the stability of **4** in DMSO since it has been shown already in the literature that this solvent is potentially problematic.[70, 71] For this purpose, the complex was dissolved in DMSO and the solution stored in the dark. After 0, 4, 8, 12, 24 and 48 h incubation, the absorption spectrum has been measured and compared. Even after 48 h (Figure S13), no significant change was observed, indicating that no decomposition occurred. As a second experiment, the stability of the compound was investigated in phosphate-buffered saline (PBS) following the same experimental protocol used for DMSO. The results (Figure 5) showed small changes in the absorption spectrum after 12 h, which increased with longer incubation times. As a third experiment, **4** was incubated in DMEM and DMEM/F-12 which are the used media for cell experiments (see section below). As expected, the absorption spectrum of the compound in DMEM (Figure S14) and DMEM/F-12 (Figure S15) did also change, suggesting a structural modification of the complex. Worthy of note, imines are well known to undergo slowly hydrolysis in an aqueous neutral solution,[72, 73] potentially explaining the decomposition of **4**.

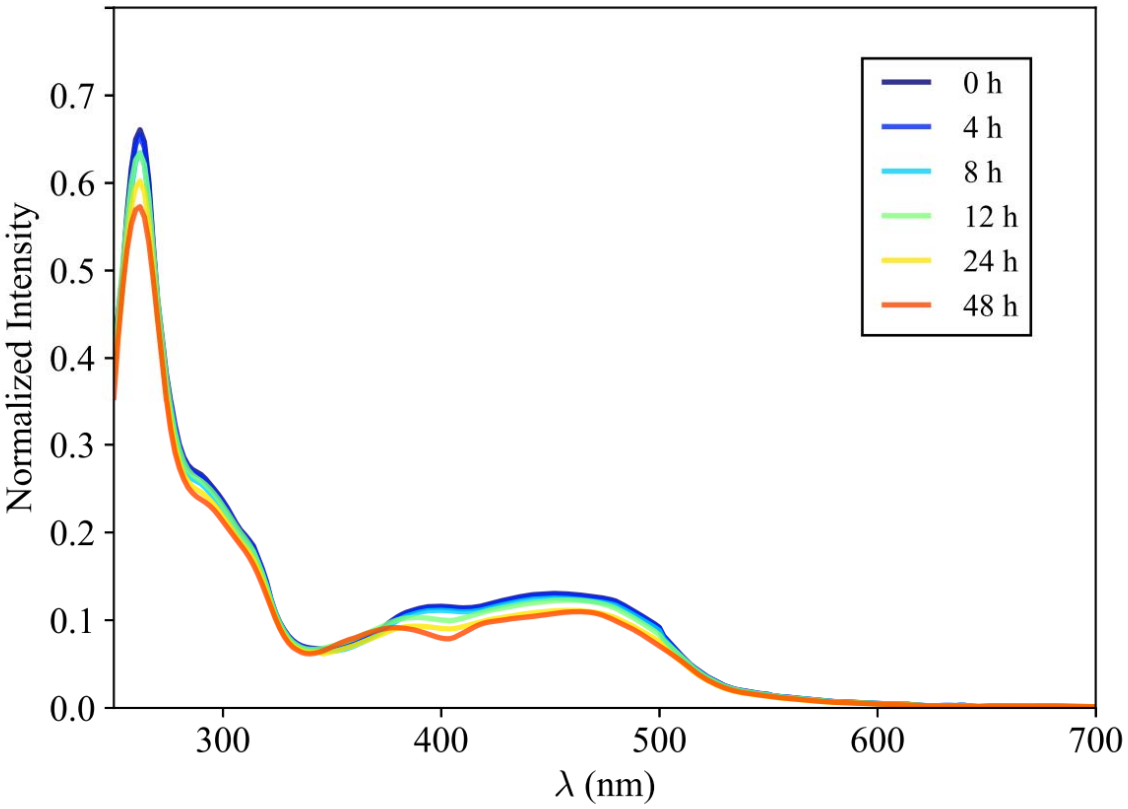

Figure 5. Temporal change of the UV/Vis spectra upon incubation of **4** in PBS.

2.7. (Photo-)cytotoxicity

We have then investigated the biological influence of **3** as well as the conjugate **4** on non-cancerous retinal pigment epithelium (RPE-1) and human cervical carcinoma (HeLa) cells. For this purpose, cells were incubated with the compounds in the dark and upon light irradiation and their cell viability determined using a fluoremetric resazurin assay. For a better evaluation of its ability, we compared **3** and **4** with the clinically approved chemotherapeutic drug cisplatin and the PDT PS Protoporphyrin IX (PpIX). The results (Table 3) show the remarkable ability of **4** to act as a PDT PS. The compound has no cytotoxic effect up to >100 µM in the dark which indicates that **4**, despite its instability in aqueous solutions, do not influence cell survival. In contrast, compound **4** showed high phototoxicity in the low micromolar range upon light exposure with a phototoxic index (PI) of up to >10.8 in HeLa and >7.3 in RPE-1 cells. A low selectivity between non-cancerous RPE-1 and cancerous HeLa cells was observed. In comparison to this, **3** had only a neglible effect with no cytotoxic effect up to >100 µM in the dark and minimal phototoxicity. Importantly, we could show that **4** was able to have a

phototoxic effect from 450 nm up to 540 nm enabling potentially higher penetration depth during PDT treatment.

Table 3. IC_{50} values in the dark and upon irradiation at 450, 480, 510 and 540 nm for **3** and **4** in comparison to cisplatin and PpIX on non-cancerous retinal pigment epithelium (RPE-1) and human cervical carcinoma (HeLa) cells. Average of three independent measurements. n.d. = not determinable.

		Dark	**450 nm (10 min, 4.7 J/cm²)**	**PI**	**480 nm (10 min, 3.1 J/cm²)**	**PI**	**510 nm (20 min, 5.0 J/cm²)**	**PI**	**540 nm (40 min, 9.5 J/cm²)**	**PI**
3	HeLa	> 100	81.3 ± 8.2	> 1.2	84.2 ± 9.5	> 1.2	> 100	n.d.	> 100	n.d.
	RPE-1	> 100	> 100	n.d.	> 100	n.d.	> 100	n.d.	> 100	n.d.
4	HeLa	> 100	18.2 ± 0.3	> 5.5	11.8 ± 0.8	> 8.5	9.3 ± 0.8	> 10.8	26.4 ± 2.1	> 3.8
	RPE-1	> 100	23.6 ± 1.0	> 4.2	17.0 ± 1.5	> 5.9	13.7 ± 1.1	> 7.3	31.3 ± 3.4	> 3.2
PpIX	HeLa	> 100	2.8 ± 0.1	> 35.7	2.5 ± 0.1	> 40.0	2.1 ± 0.3	> 47.6	2.1 ± 0.3	> 47.6
	RPE-1	> 100	4.2 ± 0.2	> 23.8	3.8 ± 0.1	> 26.3	3.1 ± 0.1	> 32.3	3.3 ± 0.1	> 30.3
Cisplatin	HeLa	10.5 ± 0.8	-	-	-	-	-	-	-	-
	RPE-1	29.3 ± 1.4	-	-	-	-	-	-	-	-

3. CONCLUSION

In summary, we were able to prepare and characterise a Ru(II) polypyridyl complex **3** bearing two aldehyde functionalities. This complex showed good photophysical properties including a strong luminescence and a high $^1O_2$ production. Importantly, **3** has a strong red shift of the MLCT transition of 35 nm towards the spectroscopic therapeutic window which enables the possibility to irradiate the PS at higher wavelengths, in comparison to its parent complex $[Ru(bipy)_3]^{2+}$. Based on the reactivity of the aldehyde groups on the ligand, as a proof of concept, we condensated **3** with benzylamine to prepare conjugate **4**. Further investigations on conjugate **4** revealed a good chemical stability in DMSO but slow degradation in an aqueous solution or cell media. Cell experiments on conjugate **4** in non-cancerous retinal pigment epithelium (RPE-1) and human cervical carcinoma (HeLa) cells showed no cytotoxicity in the dark. However, **4** was found to be highly phototoxic up to 540 nm in the low micromolar range. In comparison, **3** had only a neglible effect on the cell viability, both in the dark and upon light irradiation. Overall, we could show the potential of **3** with favourable photophysical properties and reactive aldehyde functions to act as a versatile precursor for conjugation.

4. EXPERIMENTAL SECTION

4.1. Materials

All chemicals were obtained from commercial sources and were used without further purification. Solvents were dried over molecular sieves if necessary. The Ru(II) complexes Dichlorobis(1,10-phenanthroline)ruthenium(II) $RuCl_2(phen)_2$ was synthesised as previously published using the respective ligand.[37] Dulbecco's Modified Eagles Medium (DMEM), Dulbecco's Modified Eagles Medium supplemented with nutrient mixture F-12 (DMEM/F-12), Fetal Bovine Serum (FBS), Gibco Penicillin-Streptomycin-Glutamine (Penstrep), Dulbecco's Phosphate-Buffered Saline (PBS) were purchased from Fisher Scientific and Resazurin from ACROS Organics.

4.2. Instrumentation and methods

^{1}H and ^{13}C NMR spectra were recorded on a Bruker 400 MHz NMR spectrometer. Chemical shifts (δ) are reported in parts per million (ppm) referenced to tetramethylsilane (δ 0.00) ppm using the residual proton solvent peaks as internal standards. Coupling constants (J) are reported in Hertz (Hz) and the multiplicity is abbreviated as follows: s (singlet), d (doublet), dd (doublet of doublet), m (multiplet). ESI mass spectra were recorded on a Bruker ESQUIRE-LC quadrupole ion trap spectrometer. Elemental microanalyses were performed on a LecoCHNS-932 elemental analyser.

4.3. Synthesis

4,4'-Bis(*N*,*N*-dimethylaminovinyl)-2,2'-bipyridine (**1**)

The synthesis of **1** was previously published but, in this study, another synthetic route was employed. 4,4′-Dimethyl-2,2′-bipyridine (2.00 g, 10.86 mmol, 1.0 equiv.) was dissolved in 18 mL dry DMF under N_2 atmosphere and *tert*-butoxy bis(dimethylamino)methane/Bredereck reagent (10.3 mL, 49.9 mmol, 4.6 equiv.) was added. The reaction mixture was stirred at 140 °C for 24 h. After that the orange solution was cooled to room temperature and H_2O (35 mL) was added leading to a colourless precipitate. The solid was separated by filtration and dissolved in DCM. The organic phase was dried over $MgSO_4$ and filtered. The solvent was removed by rotary evaporation and the crystalline yellow/orange product was washed with Et_2O. Yield: 79%. Experimental data fits with the literature.[36]

2,2′-Bipyridine-4,4′-dicarboxaldehyde (**2**)

The synthesis of **2** was previously published but, in this study, another synthetic route was employed. **1** (1.00 g, 3.40 mmol, 1.0 equiv.) was dissolved in 100 mL THF under N_2 atmosphere. Dropwise, a solution of $NaIO_4$ (7.27 g, 33.97 mmol, 10.0 equiv.) in 100 mL H_2O was added. The mixture was heated to 50 °C for 20 h. During this time, the formation of a white suspension was observed. After this time, the solution was cooled down to room temperature and the solvent removed. The residue was dissolved in DCM and washed with H_2O. The organic phase was dried over $MgSO_4$, filtered and the solvent was removed by rotary evaporation. The product was dissolved in DCM and isolated by precipitation from pentane. The solid was obtained by filtration as a pale yellow solid. Yield: 78%. Experimental data fits with the literature.[36]

(2,2′-Bipyridine-4,4′-dicarboxaldehyde)bis(1,10-phenanthroline)ruthenium(II)

hexafluorophosphate (**3**)

$RuCl_2(phen)_2$ (150 mg, 0.28 mmol, 1.0 equiv.) and **2** (66 mg, 0.31 mmol, 1.1 equiv.) were dissolved in a 1:1 mixture of H_2O/EtOH (20 mL) and were refluxed for 18 h under N_2 atmosphere. The solvent was evaporated by rotary evaporation and the residue redissolved in 5 mL of H_2O. A saturated, aq. NH_4PF_6 solution was added and the resulting precipitate was collected by vacuum filtration. The solid was washed with H_2O (50 mL) and Et_2O (50 mL). The product was purified twice by column chromatography on silica gel with an CH_3CN /aq. KNO_3 (0.4 M) solution (10:1) and (20:1). The fractions containing the product were united and the solvent was removed. The residue was dissolved in CH_3CN and undissolved KNO_3 was removed by filtration. The solvent was removed and the product was dissolved in H_2O (50 mL). Upon addition of NH_4PF_6 the product precipitated as a PF_6 salt. The solid was obtained by filtration and was washed with H_2O (50 mL) and Et_2O (50 mL). The product was dried in high vacuum. Yield: 69%. ^{1}H NMR (400 MHz, CD_3CN) δ = 10.17 (2H, s), 9.04 (2H, dd, J = 1.8 Hz, 0.8 Hz), 8.69 (2H, dd, J = 8.3 Hz, 1.3 Hz), 8.60 (2H, dd, J = 8.3 Hz, 1.3 Hz), 8.29-8.24 (4H, m), 8.15 (2H, dd, J = 5.3, 1.3 Hz), 7.99 (2H, d, J = 5.8 Hz), 7.87 (2H, dd, J = 5.3, 1.3 Hz), 7.78 (2H, dd, J = 8.3 Hz, 5.3 Hz), 7.66 (2H, dd, J = 5.8, 1.7 Hz), 7.60 (2H, dd, J = 8.3, 5.3 Hz). ^{13}C NMR (100 MHz, CD_3CN) δ = 191.3, 159.6, 155.0, 153.9, 153.5, 148.5, 148.1, 143.0, 138.5, 138.3, 132.1, 132.1, 129.1, 129.1, 127.1, 127.1, 126.5, 123.9. HR-MS (ESI + m/z): Calcd. [M-2PF 6 +2MeOH] 2+ : 369. 07588; found: 369.07601. EA (%): Calcd. for ($C_{36}H_{24}F_{12}N_6P_2O_2Ru$): C 44.87, H 2.51, N 8.72; found: C 44.72, H 2.57, N 8.62.

(4,4'-Bis(*N*-Benzylimine)-2,2'-bipyridine)bis(1,10-phenanthroline)ruthenium(II) hexafluorophosphate (**4**)

3 (100 mg, 0.10 mmol, 1.0 equiv.) was dissolved in dry EtOH (30 mL) and benzylamine (113 µL, 1.04 mmol, 10.0 equiv.) was added dropwise to this solution. The reaction mixture was heated at 50 °C for 2 h. After this time, the solution was cooled down to room temperature and the product precipitated upon addition of Et_2O. The resulting solid was collected via centrifugation. The product was washed with Et_2O and pentane. The product was isolated via fractionated precipitation from CH_3CN by adding dropwise Et_2O. The product was dried in high vacuum. Yield: 54 %. ^{1}H NMR (400 MHz, CD_3CN) δ = 8.85 (2H, d, J = 0.9 Hz), 8.66 (2H, dd, J = 8.2 Hz, 1.0 Hz), 8.59-8.52 (m, 4H), 8.29-8.18 (m, 8H), 7.87 (2H, dd, J = 5.1, 1.1 Hz), 7.79-73 (m, 4H), 7.59-7.54 (m, 6H), 7.38-7.34 (m, 6H), 7.31-7.27 (m, 2H), 4.89 (s, 2H), 13C NMR (100 MHz, CD3CN) δ = 159.5, 158.8, 153.9, 153.7, 153.5, 148.7, 148.3, 145.4, 139.6, 138.0, 137.9, 132.0, 132.0, 129.5, 129.2, 129.0, 128.2, 127.0, 126.9, 125.9, 123.1, 65.6. MS (ESI +) m/z: Calcd. [M]2+ : 426.1; found: 426.4, Calcd. [M-PF6]+ : 997.2; found: 998.0.

4.4. X-ray crystallography

The single-crystal Xray diffraction studies were carried out at 183(1) K on a Rigaku OD SuperNova diffractometer (CCD Atlas detector) for **3a** and on a Rigaku OD XtaLAB Synergy Dualflex diffractometer (Pilatus 200K detector) for **3b**, using Oxford liquid-nitrogen cryostream coolers. Single wavelength X-ray sources from micro-focus sealed X-ray tubes were used with the Mo K_α radiation (λ = 0.71073 Å)[74] for **3a** and with the Cu K_α radiation (λ = 1.54184 Å)[74] for **3b**. The selected single crystals were mounted on a flexible loop using polybutene oil fixed on a goniometer head and transferred to the diffractometer. Pre-experiments, data collections, data reductions and analytical absorption corrections[75] were performed with the program suite *CrysAlisPro*.[76] Using *Olex2*,[77] the structures were solved with the *SHELXT*[78] small molecule structure solution program and refined with the *SHELXL* program package[79] by full-matrix least-squares minimization on F^2. The representations of the molecular structures were generated using *Mercury 4.0.[80]* CCDC 1891337 (**3b**) and 1891338 (**3a**) contain the supplementary crystallographic data for these compounds, and can be obtained free of charge from the Cambridge Crystallographic Data Centre via www.ccdc.cam.ac.uk/data_request/cif.

4.5. Spectroscopic measurements

The absorption of the samples has been measured with a SpectraMax M2 Spectrometer (Molecular Devices). The emission was measured by irradiation of the sample in fluorescence quartz cuvettes (width 1 cm) using a NT342B Nd-YAG pumped optical parametric oscillator (Ekspla) at 355 nm. Luminescence was focused and collected at right angle to the excitation pathway and directed to a Princeton Instruments Acton SP-2300i monochromator. As a detector a XPI-Max 4 CCD camera (Princeton Instruments) has been used.

4.6. Luminescence quantum yield measurements

For the determination of the luminescence quantum yield, the samples were prepared in an CH_3CN solution with an absorbance of 0.1 at 355 nm. This solution was irradiated in fluorescence quartz cuvettes (width 1 cm) using a NT342B Nd-YAG pumped optical parametric oscillator (Ekspla) at 355 nm. The emission signal was focused and collected at right angle to the excitation pathway and directed to a Princeton Instruments Acton SP-2300i monochromator. As a detector a XPI-Max 4 CCD camera (Princeton Instruments) has been used. The luminescence quantum yields were determined by comparison with the reference $[Ru(bipy)_3]Cl_2$ in CH_3CN (Φ_{em}=5.9%)[46] applying the following formula:

$$\Phi_{em,\,sample} = \Phi_{em,\,reference} * (F_{reference} / F_{sample}) * (I_{sample} / I_{reference}) * (n_{sample} / n_{reference})^2$$

$$F = 1 - 10^{-A}$$

Φ_{em} = luminescence quantum yield, F = fraction of light absorbed, I = integrated emission intensities, n = refractive index, A = absorbance of the sample at irradiation wavelength.

4.7. Lifetime measurements

For the determination of the lifetimes, the samples were prepared in an air saturated and in a degassed CH_3CN solution with an absorbance of 0.1 at 355 nm. This solution was irradiated in fluorescence quartz cuvettes (width 1 cm) using a NT342B Nd-YAG pumped optical parametric oscillator (Ekspla) at 355 nm. The emission signal was focused and collected at right angle to the excitation pathway and directed to a Princeton Instruments Acton SP-2300i monochromator. As a detector a R928 photomultiplier tube (Hamamatsu) has been used.

4.8. Computational Details

All calculations were performed using the Gaussian 09 software package [81]. All calculations were performed using Density Functional Theory (DFT) and Time Dependent DFT (TD-DFT) to characterize ground or excited states, respectively. Solvent effects were included using an implicit model (i.e. the Polarizable Continuum Model - PCM [82]). In line with available experimental data, acetonitrile was considered as solvent. All calculations were performed using the global hybrid functional PBE0[83] in conjunction with the Los Alamos LANL2[84] effective core potential and the corresponding double-zeta basis set for the Ruthenium atom, with all other atoms treated with the Pople[85] double-zeta basis set with a single set of polarisation[86, 87] functions on non-hydrogen atoms (6-31G(d)).

Ground state (singlet) structure of **3** was fully optimized and its nature (minimum) was checked by a subsequent frequency calculation. Vertical transition energies were obtained at the same level of theory for the first 60 excited states in order to cover the spectral range of interest, that is up to roughly 250 nm). Absorption spectra were simulated by convolution with Gaussian functions with a full width at half maximum (FWHM) of 0.4 eV. In order to characterize the nature of the lowest energy states possessing a non-negligible intensity (that is an oscillator strength, f, > 0.1 a.u.) unrelaxed excited state density was also computed together with the corresponding associated charge transfer distance (D_{CT}) following the procedure described in ref[43-45].

4.9. Singlet oxygen measurements

- **Direct evaluation**

The samples were prepared in an air saturated CH_3CN or D_2O solution with an absorbance of 0.2 at 450 nm. This solution was irradiated in fluorescence quartz cuvettes (width 1 cm) using a mounted M450LP1 LED (Thorlabs) whose irradiation, centered at 450 nm, has been focused with aspheric condenser lenses. The intensity of the irradiation has been varied using a T-Cube LED Driver (Thorlabs) and measured with an optical power and energy meter. The emission signal was focused and collected at right angle to the excitation pathway and directed to a Princeton Instruments Acton SP-2300i monochromator. A longpass glass filter was placed in front of the monochromator entrance slit to cut off light at wavelengths shorter than 850 nm. As a detector an EO-817L IR-sensitive liquid nitrogen cooled germanium diode detector (North Coast Scientific Corp.) has been used. The singlet oxygen luminesce at 1270 nm was measured by recording spectra from 1100 to 1400 nm. For the data analysis, the singlet oxygen luminescence peaks at different irradiation intensities were integrated. The resulting areas were

plotted against the percentage of the irradiation intensity and the slope of the linear regression calculated. The absorbance of the sample was corrected with an absorbance correction factor. As reference for the measurement in an CH_3CN solution phenalenone ($\Phi_{phenaleone}$=95%)[52] and for the measurement in a D_2O solution $[Ru(bipy)_3]Cl_2$ ($\Phi_{Ru(bipy)3Cl2}$=22%)[47] was used and the singlet oxygen quantum yields were calculated using the following formula:

$\Phi_{sample} = \Phi_{reference} * (S_{sample} / S_{reference}) * (I_{reference} / I_{sample})$

$I = I_0 * (1 - 10^{-A})$

Φ = singlet oxygen quantum yield, S = slope of the linear regression of the plot of the areas of the singlet oxygen luminescence peaks against the irradiation intensity, I = absorbance correction factor, I0 = light intensity of the irradiation source, A = absorbance of the sample at irradiation wavelength.

- **Indirect evaluation**

For the measurement in CH_3CN: The samples were prepared in an air-saturated CH_3CN solution containing the complex with an absorbance of 0.2 at the irradiation wavelength, *N*,*N*-dimethyl-4-nitrosoaniline aniline (RNO, 24 µM) and imidazole (12 mM). For the measurement in PBS buffer: The samples were prepared in an air-saturated PBS solution containing the complex with an absorbance of 0.1 at the irradiation wavelength, *N*,*N*-dimethyl-4-nitrosoaniline aniline (RNO, 20 µM) and histidine (10 mM). The samples were irradiated on 96 well plates with an Atlas Photonics LUMOS BIO irradiator for different times. The absorbance of the samples was measured during these time intervals with a SpectraMax M2 Microplate Reader (Molecular Devices). The difference in absorbance (A0-A) at 420 nm for the CH_3CN solution or at 440 nm a PBS buffer solution was calculated and plotted against the irradiation times. From the plot the slope of the linear regression was calculated as well as the absorbance correction factor determined. The singlet oxygen quantum yields were calculated using the same formulas as used for the direct evaluation.

4.10. Stability measurements

The stability of the compound in DMSO/PBS/DMEM/DMEM-F12 was determined by UV/Vis spectroscopy. The compound was dissolved and stored at room temperature in the dark. The absorption spectrum from 250-650 nm was recorded with a SpectraMax M2 Microplate Reader (Molecular Devices) after each time interval (0, 4, 8, 12, 24, 48 h) and compared.

4.11. Cell culture

Human cervical carcinoma (HeLa) cells were cultured using DMEM media and retinal pigment epithelium (RPE-1) cells using DMEM/F-12 with addition of 10% FBS and 1% penstrep. The cells were cultivated and maintained at 37 °C in a cell culture incubator at 37 °C with 5% CO_2 atmosphere. Before an experiment, the cells were passaged three times.

4.12. (Photo-)cytotoxicity

The cytotoxicity of the compounds was assessed by measuring cell viability using a fluorometric resazurin assay. The cultivated cells were seeded in triplicates in 96 well plates with a density of 4000 cells per well in 100 µL of media. After 24 h, the medium was removed and the cells were treated with increasing concentrations of the compound diluted in cell media achieving a total volume of 200 µL. The cells were incubated with the compound for 4 h. After this time, the media was removed and replaced with 200 µL of fresh medium. For the phototoxicity studies, the cells were exposed to light with an Atlas Photonics LUMOS BIO irradiator. Each well was constantly illuminated with either a 480 nm or 510 nm irradiation. During this time, the temperature was maintained constantly at 37 °C. The cells were grown in the incubator for additional 44 h. For the determination of the dark cytotoxicity, the cells were not irradiated and after the medium exchange directly incubated for 44 h. After this time, the medium was replaced with fresh medium containing resazurin with a final concentration of 0.2 mg/mL. After 4 h incubation, the amount of the fluorescent product resorufin was determined upon excitation at 540 nm and measurement its emission at 590 nm using a SpectraMax M2 Microplate Reader (Molecular Devices). The obtained data was analyzed with the GraphPad Prism software.

ACKNOWLEDGEMENTS

This work was financially supported by an ERC Consolidator Grant PhotoMedMet to G.G. (GA 681679) and has received support under the program “Investissements d’Avenir” launched by the French Government and implemented by the ANR with the reference ANR-10-IDEX-0001-02 PSL (G.G.). FH, OB and BS thank for support by the University of Zurich. We thank Dr. Philippe Goldner for access to state-of-the-art laser apparatus. I.C and F.M. gratefully acknowledge the European Research Council (ERC) for funding (ERC Consolidator Grant STRIGES to I.C., GA No 648558).

REFERENCES

[1] A.E. O'Connor, W.M. Gallagher, A.T. Byrne, Porphyrin and nonporphyrin photosensitizers in oncology: preclinical and clinical advances in photodynamic therapy, Photochem. Photobiol., 85 (2009) 1053-1074.

[2] R. Bonnett, Photosensitizers of the porphyrin and phthalocyanine series for photodynamic therapy, Chem. Soc. Rev., 24 (1995) 19-33.

[3] D.E. Dolmans, D. Fukumura, R.K. Jain, Photodynamic therapy for cancer, Nat. Rev. Cancer, 3 (2003) 380-387.

[4] M. Ethirajan, Y. Chen, P. Joshi, R.K. Pandey, The role of porphyrin chemistry in tumor imaging and photodynamic therapy, Chem. Soc. Rev., 40 (2011) 340-362.

[5] F. Heinemann, J. Karges, G. Gasser, Critical Overview of the Use of Ru (II) Polypyridyl Complexes as Photosensitizers in One-Photon and Two-Photon Photodynamic Therapy, Acc. Chem. Res., 50 (2017) 2727-2736.

[6] C. Mari, V. Pierroz, S. Ferrari, G. Gasser, Combination of Ru(ii) complexes and light: new frontiers in cancer therapy, Chem. Sci., 6 (2015) 2660-2686.

[7] M. Jakubaszek, B. Goud, S. Ferrari, G. Gasser, Mechanisms of action of Ru (II) polypyridyl complexes in living cells upon light irradiation, Chem. Commun., 54 (2018) 13040-13059.

[8] S. Monro, K.L. Colón, H. Yin, J. Roque III, P. Konda, S. Gujar, R.P. Thummel, L. Lilge, C.G. Cameron, S.A. McFarland, Transition Metal Complexes and Photodynamic Therapy from a Tumor-Centered Approach: Challenges, Opportunities, and Highlights from the Development of TLD1433, Chem. Rev., 119 (2019) 797-828.

[9] L. Zeng, P. Gupta, Y. Chen, E. Wang, L. Ji, H. Chao, Z.-S. Chen, The development of anticancer ruthenium (II) complexes: from single molecule compounds to nanomaterials, Chem. Soc. Rev., 46 (2017) 5771-5804.

[10] J. Liu, C. Zhang, T.W. Rees, L. Ke, L. Ji, H. Chao, Harnessing ruthenium (II) as photodynamic agents: Encouraging advances in cancer therapy, Coord. Chem. Rev., 363 (2018) 17-28.

[11] L.K. McKenzie, H.E. Bryant, J.A. Weinstein, Transition metal complexes as photosensitisers in one-and two-photon photodynamic therapy, Coord. Chem. Rev., 379 (2019) 2-29.

[12] H. Huang, B. Yu, P. Zhang, J. Huang, Y. Chen, G. Gasser, L. Ji, H. Chao, Highly Charged Ruthenium (II) Polypyridyl Complexes as Lysosome-Localized Photosensitizers for Two-Photon Photodynamic Therapy, Angew. Chem. Int. Ed., 54 (2015) 14049-14052.

[13] C. Mari, V. Pierroz, R. Rubbiani, M. Patra, J. Hess, B. Spingler, L. Oehninger, J. Schur, I. Ott, L. Salassa, DNA intercalating RuII polypyridyl complexes as effective photosensitizers in photodynamic therapy, Chem. Eur. J., 20 (2014) 14421-14436.

[14] C. Mari, V. Pierroz, A. Leonidova, S. Ferrari, G. Gasser, Towards Selective Light-Activated RuII-Based Prodrug Candidates, Eur. J. Inorg. Chem., 2015 (2015) 3879-3891.

[15] C. Mari, V. Pierroz, S. Ferrari, G. Gasser, Combination of Ru (II) complexes and light: new frontiers in cancer therapy, Chem. Sci., 6 (2015) 2660-2686.

[16] L. Tabrizi, H. Chiniforoshan, New Ru II pincer complexes: synthesis, characterization and biological evaluation for photodynamic therapy, Dalton Trans., 45 (2016) 18333-18345.

[17] Y. Lu, R. Conway-Kenny, B. Twamley, N. McGoldrick, J. Zhao, S.M. Draper, 1, 10-Phenanthroline Ruthenium (II) Complexes as Model Systems in the Search for High-Performing Triplet Photosensitisers: Addressing Ligand versus Metal Effects, ChemPhotoChem, 1 (2017) 544-552.

[18] L. Wang, H. Yin, M.A. Jabed, M. Hetu, C. Wang, S. Monro, X. Zhu, S. Kilina, S.A. McFarland, W. Sun, π-Expansive Heteroleptic Ruthenium (II) Complexes as Reverse Saturable Absorbers and Photosensitizers for Photodynamic Therapy, Inorg. Chem., 56 (2017) 3245-3259.
[19] M. Grätzel, Dye-sensitized solar cells, J. Photochem. Photobiol. C, 4 (2003) 145-153.
[20] M. Eriksson, M. Leijon, C. Hiort, B. Norden, A. Graeslund, Binding of delta and lambda $[Ru(phen)_3]^{2+}$ to $[d(CGCGATCGCG)]_2$ studied by NMR, Biochemistry, 33 (1994) 5031-5040.
[21] M. Eriksson, M. Leijon, C. Hiort, B. Norden, A. Graeslund, Minor groove binding of $[Ru(phen)_3]^{2+}$ to $[d(CGCGATCGCG)]_2$ evidenced by two-dimensional NMR, J. Am. Chem. Soc., 114 (1992) 4933-4934.
[22] C. Mari, R. Rubbiani, G. Gasser, Biological evaluation of nitrile containing Ru(II) polypyridyl complexes as potential photodynamic therapy agents, Inorg. Chim. Acta, 454 (2017) 21-26.
[23] J. Hess, H. Huang, A. Kaiser, V. Pierroz, O. Blacque, H. Chao, G. Gasser, Evaluation of the Medicinal Potential of Two Ruthenium (II) Polypyridine Complexes as One-and Two-Photon Photodynamic Therapy Photosensitizers, Chem. Eur. J., (2017) 9888-9896.
[24] C.M. Anderson, I.R. Taylor, M.F. Tibbetts, J. Philpott, Y. Hu, J.M. Tanski, Hetero-multinuclear ruthenium (III)/platinum (II) complexes that potentially exhibit both antimetastatic and antineoplastic properties, Inorg. Chem., 51 (2012) 12917-12924.
[25] S.L. Higgins, A.J. Tucker, B.S. Winkel, K.J. Brewer, Metal to ligand charge transfer induced DNA photobinding in a Ru (II)–Pt (II) supramolecule using red light in the therapeutic window: a new mechanism for DNA modification, Chem. Commun., 48 (2012) 67-69.
[26] R. Miao, M.T. Mongelli, D.F. Zigler, B.S. Winkel, K.J. Brewer, A multifunctional tetrametallic Ru− Pt supramolecular complex exhibiting both DNA binding and photocleavage, Inorg. Chem., 45 (2006) 10413-10415.
[27] C.A. Puckett, J.K. Barton, Fluorescein redirects a ruthenium− octaarginine conjugate to the nucleus, J. Am. Chem. Soc., 131 (2009) 8738-8739.
[28] M. Dickerson, Y. Sun, B. Howerton, E.C. Glazer, Modifying charge and hydrophilicity of simple Ru (II) polypyridyl complexes radically alters biological activities: old complexes, surprising new tricks, Inorg. Chem., 53 (2014) 10370-10377.
[29] T. Wang, N. Zabarska, Y. Wu, M. Lamla, S. Fischer, K. Monczak, D.Y. Ng, S. Rau, T. Weil, Receptor selective ruthenium-somatostatin photosensitizer for cancer targeted photodynamic applications, Chem. Commun., 51 (2015) 12552-12555.
[30] J. Lee, D.G. Udugamasooriya, H.-S. Lim, T. Kodadek, Potent and selective photo-inactivation of proteins with peptoid-ruthenium conjugates, Nat. Chem. Biol., 6 (2010) 258-260.
[31] M.A. Sprung, A Summary of the Reactions of Aldehydes with Amines, Chem. Rev., 26 (1940) 297-338.
[32] E. Ashby, Grignard reagents. Compositions and mechanisms of reaction, Q. Rev. Chem. Soc., 21 (1967) 259-285.
[33] D. Chen, M.M. Disotuar, X. Xiong, Y. Wang, D.H.-C. Chou, Selective N-terminal functionalization of native peptides and proteins, Chem. Sci., 8 (2017) 2717-2722.
[34] H.F. Gaertner, R.E. Offord, Site-specific attachment of functionalized poly (ethylene glycol) to the amino terminus of proteins, Bioconjugate Chem., 7 (1996) 38-44.
[35] S.S. Mark, Bioconjugation Protocols, Springer Protocols, 2004.
[36] O. Maury, J.-P. Guégan, T. Renouard, A. Hilton, P. Dupau, N. Sandon, L. Toupet, H. Le Bozec, Design and synthesis of 4, 4′-π-conjugated [2, 2′]-bipyridines: a versatile class of tunable chromophores and fluorophores, New J. Chem., 25 (2001) 1553-1566.

[37] B. Sullivan, D. Salmon, T. Meyer, Mixed phosphine 2, 2'-bipyridine complexes of ruthenium, Inorg. Chem., 17 (1978) 3334-3341.
[38] B. Spingler, S. Schnidrig, T. Todorova, F. Wild, Some thoughts about the single crystal growth of small molecules, CrystEngComm, 14 (2012) 751-757.
[39] A.L. Spek, PLATON SQUEEZE: a tool for the calculation of the disordered solvent contribution to the calculated structure factors, Acta Crystallographica Section C: Structural Chemistry, 71 (2015) 9-18.
[40] C.W. Stark, W.J. Schreier, J. Lucon, E. Edwards, T. Douglas, B. Kohler, Interligand electron transfer in heteroleptic ruthenium (II) complexes occurs on multiple time scales, J. Phys. Chem. A, 119 (2015) 4813-4824.
[41] A. Juris, V. Balzani, F. Barigelletti, S. Campagna, P. Belser, A. von Zelewsky, Ru (II) polypyridine complexes: photophysics, photochemistry, eletrochemistry, and chemiluminescence, Coord. Chem. Rev., 84 (1988) 85-277.
[42] S. Campagna, F. Puntoriero, F. Nastasi, G. Bergamini, V. Balzani, Photochemistry and Photophysics of Coordination Compounds: Ruthenium, in: V. Balzani, S. Campagna (Eds.) Photochemistry and Photophysics of Coordination Compounds I, Springer Berlin Heidelberg, Berlin, Heidelberg, 2007, pp. 117-214.
[43] T. Le Bahers, C. Adamo, I. Ciofini, A qualitative index of spatial extent in charge-transfer excitations, J. Chem. Theory Comput., 7 (2011) 2498-2506.
[44] F. Maschietto, M. Campetella, M.J. Frisch, G. Scalmani, C. Adamo, I. Ciofini, How are the charge transfer descriptors affected by the quality of the underpinning electronic density?, J. Comput. Chem., 39 (2018) 735-742.
[45] J. Sanz García, F. Maschietto, M. Campetella, I. Ciofini, Using Density Based Indexes and Wave Function Methods for the Description of Excited States: Excited State Proton Transfer Reactions as a Test Case, J. Phys. Chem. A, 122 (2018) 375-382.
[46] K. Nakamaru, Solvent Effect on the Nonradiative Deactivation of the Excited State of Tris(2,2′-bipyridyl)ruthenium(II) Ion, Bull. Chem. Soc. Jpn., 55 (1982) 1639-1640.
[47] D. Garcìa-Fresnadillo, Y. Georgiadou, G. Orellana, A.M. Braun, E. Oliveros, Singlet-Oxygen (1Δg) Production by Ruthenium (II) complexes containing polyazaheterocyclic ligands in methanol and in water, Helv. Chim. Acta, 79 (1996) 1222-1238.
[48] A.A. Abdel-Shafi, P.D. Beer, R.J. Mortimer, F. Wilkinson, Photosensitized generation of singlet oxygen from (substituted bipyridine) ruthenium (II) complexes, Helv. Chim. Acta, 84 (2001) 2784-2795.
[49] K. Nakamaru, Synthesis, luminescence quantum yields, and lifetimes of trischelated ruthenium (II) mixed-ligand complexes including 3, 3′-dimethyl-2, 2′-bipyridyl, Bull. Chem. Soc. Jpn., 55 (1982) 2697-2705.
[50] Y. Ellahioui, M. Patra, C. Mari, R. Kaabi, J. Karges, G. Gasser, S. Gómez-Ruiz, Mesoporous silica nanoparticles functionalised with a photoactive ruthenium (ii) complex: exploring the formulation of a metal-based photodynamic therapy photosensitiser, Dalton Trans., (2019), DOI: 10.1039/C8DT02392A.
[51] J. Karges, P. Goldner, G. Gasser, Synthesis, Characterization, and Biological Evaluation of Red-Absorbing Fe (II) Polypyridine Complexes, Inorganics, 7 (2019) 4.
[52] I.E. Kochevar, R.W. Redmond, Photosensitized production of singlet oxygen, Methods Enzymol., Academic Press 2000, pp. 20-28.
[53] M. Islam, M. Razzak, M. Karim, A.H. Mirza, H-bond plays key role in the synthesis of stable hemiaminals, Tetrahedron Lett., 58 (2017) 1429-1432.
[54] F. Cheng, S. Yu, M. Ren, C. He, H. Yin, Di-and trinuclear Ru (II) complexes of 1, 10-phenanthroline and 2, 2′-bipyridine derivatives; synthesis, photophysical and electrochemical properties, Transition Met. Chem., 41 (2016) 305-314.

[55] J. González-García, À. Martínez-Camarena, B. Verdejo, M.P. Clares, C. Soriano, E. García-España, H.R. Jiménez, A. Doménech-Carbó, R. Tejero, E. Calvo, Oxidative stress protection by manganese complexes of tail-tied aza-scorpiand ligands, J. Inorg. Biochem., 163 (2016) 230-239.
[56] A. Ramdass, V. Sathish, M. Velayudham, P. Thanasekaran, S. Umapathy, S. Rajagopal, Synthesis and characterization of monometallic rhenium (I) complexes and their application as selective sensors for copper (II) ions, RSC Adv., 5 (2015) 38479-38488.
[57] S. Gago, J. González, S. Blasco, A.J. Parola, M. Albelda, E. García-España, F. Pina, Protonation, coordination chemistry, cyanometallate "supercomplex" formation and fluorescence chemosensing properties of a bis (2, 2′-bipyridino) cyclophane receptor, Dalton Trans., 43 (2014) 2437-2447.
[58] M. Strelkov, R. Zaripov, V. Dzhabarov, A. Knyazev, K. Salikhov, V. Voronkova, Y.G. Galyametdinov, Structure of the Ln III tris (β-diketonate) adduct with substituted bipyridine determined by the ESR and computer simulation data, Russ. Chem. Bull., 57 (2008) 1564-1567.
[59] L. Peng, C. Chen, C.R. Gonzalez, V. Balogh-Nair, Bioorganic studies in AIDS: synthetic antifungals against Pneumocystis carinii based on the multivalency concept, Int. J. Mol. Sci., 3 (2002) 1145-1161.
[60] H. Oh, J. Kim, S.H. Yun, J. Lee, B. Park, J. Tak, B.H. Kim, Synthesis of heteroleptic Ru (II) complexes ligated with 1, 3-dihydro-1, 1, 3, 3-tetramethyl-7, 8-diazacyclopenta [1] phenanthren-2-one and application in dye-sensitized solar cells, Synth. Met., 198 (2014) 260-266.
[61] J. Tak, M. Kim, S. Park, S.H. Yun, J. Kim, B. Park, B.H. Kim, Synthesis and photophysical properties of new ruthenium (II) charge-transfer sensitizers containing a 4, 7-bis (E-carboxyvinyl)-1,10-phenanthroline ligand, Monatsh. Chem., 145 (2014) 1101-1108.
[62] D. Chao, W.-F. Fu, Facile synthesis of a ruthenium assembly and its application for light-driven oxidation of alcohols in water, Chem. Commun., 49 (2013) 3872-3874.
[63] C. Klein, M.K. Nazeeruddin, P. Liska, D. Di Censo, N. Hirata, E. Palomares, J. Durrant, M. Grätzel, Engineering of a novel ruthenium sensitizer and its application in dye-sensitized solar cells for conversion of sunlight into electricity, Inorg. Chem., 44 (2005) 178-180.
[64] L.D. Ciana, W.J. Dressick, A. Von Zelewsky, Synthesis of 4, 4′-divinyl-2, 2′-bipyridine, J. Heterocycl. Chem., 27 (1990) 163-165.
[65] S. Gouthaman, S. Periyaraja, P. Shanmugam, Bipyridine carbaldehydes as electrophiles in the Morita–Baylis–Hillman reaction: synthesis of highly functionalized bipyridyl ligands and a macrocycle, Tetrahedron Lett., 56 (2015) 5920-5923.
[66] G. Konti, G.C. Vougioukalakis, M. Bidikoudi, A.G. Kontos, C. Methenitis, P. Falaras, A Ru (II) molecular antenna bearing a novel bipyridine–acrylonitrile ligand: Synthesis and application in dye solar cells, Polyhedron, 82 (2014) 12-18.
[67] B.J. Coe, J. Fielden, S.P. Foxon, B.S. Brunschwig, I. Asselberghs, K. Clays, A. Samoc, M. Samoc, Combining very large quadratic and cubic nonlinear optical responses in extended, tris-chelate metallochromophores with six π-conjugated pyridinium substituents, J. Am. Chem. Soc., 132 (2010) 3496-3513.
[68] B.S. Jursic, D.M. Neumann, Preparation of 5, 5′-pyrilidene and 5, 5′-quinolidene bis-barbituric acid derivatives, J. Heterocycl. Chem., 40 (2003) 465-474.
[69] Z. Mao, M. Wang, J. Liu, L.-J. Liu, S.M.-Y. Lee, C.-H. Leung, D.-L. Ma, A long lifetime switch-on iridium (III) chemosensor for the visualization of cysteine in live zebrafish, Chem. Commun., 52 (2016) 4450-4453.

[70] M. Patra, T. Joshi, V. Pierroz, K. Ingram, M. Kaiser, S. Ferrari, B. Spingler, J. Keiser, G. Gasser, DMSO-Mediated Ligand Dissociation: Renaissance for Biological Activity of N-Heterocyclic-[Ru (η6-arene)Cl_2] Drug Candidates, Chem. Eur. J., 19 (2013) 14768-14772.
[71] M.D. Hall, K.A. Telma, K.-E. Chang, T.D. Lee, J.P. Madigan, J.R. Lloyd, I.S. Goldlust, J.D. Hoeschele, M.M. Gottesman, Say no to DMSO: dimethylsulfoxide inactivates cisplatin, carboplatin, and other platinum complexes, Cancer Res., 74 (2014) 3913-3922.
[72] C. Godoy-Alcántar, A.K. Yatsimirsky, J.M. Lehn, Structure-stability correlations for imine formation in aqueous solution, J. Phys. Org. Chem., 18 (2005) 979-985.
[73] R.W. Layer, The Chemistry of Imines, Chem. Rev., 63 (1963) 489-510.
[74] Rigaku Oxford Diffraction, (2015).
[75] R. Clark, J. Reid, The analytical calculation of absorption in multifaceted crystals, Acta Crystallogr. Sect. A: Found. Crystallogr., 51 (1995) 887-897.
[76] CrysAlisPro (version 1.171.39.13a), Rigaku Oxford Diffraction, (2016).
[77] O.V. Dolomanov, L.J. Bourhis, R.J. Gildea, J.A.K. Howard, H. Puschmann, OLEX2: a complete structure solution, refinement and analysis program, J. Appl. Crystallogr., 42 (2009) 339-341.
[78] G.M. Sheldrick, SHELXT–Integrated space-group and crystal-structure determination, Acta Crystallographica Section A: Foundations and Advances, 71 (2015) 3-8.
[79] G.M. Sheldrick, Crystal structure refinement with SHELXL, Acta Crystallographica Section C: Structural Chemistry, 71 (2015) 3-8.
[80] C.F. Macrae, P.R. Edgington, P. McCabe, E. Pidcock, G.P. Shields, R. Taylor, M. Towler, J.v.d. Streek, Mercury: visualization and analysis of crystal structures, J. Appl. Crystallogr., 39 (2006) 453-457.
[81] Gaussian: Frisch, M. J.; et al. Gaussian 16; Gaussian, Inc.: Wallingford, CT, **2017**.
[82] A. Klamt, C. Moya, J. Palomar, A comprehensive comparison of the IEFPCM and SS (V) PE continuum solvation methods with the COSMO approach, J. Chem. Theory Comput., 11 (2015) 4220-4225.
[83] C. Adamo, V. Barone, Toward reliable density functional methods without adjustable parameters: The PBE0 model, J. Chem. Phys., 110 (1999) 6158-6170.
[84] T. H. Dunning Jr. and P. J. Hay, in *Modern Theoretical Chemistry*, Ed. H. F. Schaefer III, Vol. 3 (Plenum, New York, **1977**) 1-28.
[85] W.J. Hehre, R. Ditchfield, J.A. Pople, Self—consistent molecular orbital methods. XII. Further extensions of Gaussian—type basis sets for use in molecular orbital studies of organic molecules, J. Chem. Phys., 56 (1972) 2257-2261.
[86] P.C. Hariharan, J.A. Pople, The influence of polarization functions on molecular orbital hydrogenation energies, Theor. Chim. Acta, 28 (1973) 213-222.
[87] M.M. Francl, W.J. Pietro, W.J. Hehre, J.S. Binkley, M.S. Gordon, D.J. DeFrees, J.A. Pople, Self-consistent molecular orbital methods. XXIII. A polarization-type basis set for second-row elements, J. Chem. Phys., 77 (1982) 3654-3665.